



Cite this: *RSC Adv.*, 2020, 10, 34800

# Thermal property and structural molecular dynamics of organic–inorganic hybrid perovskite 1,4-butanediammonium tetrachlorocuprate †

Ma Byong Yoon,<sup>a</sup> Won Jun Lee<sup>b</sup> and Ae Ran Lim  <sup>\*ac</sup>

We investigate the thermal behaviour and physical properties of the crystals of the organic inorganic hybrid perovskite  $[(\text{NH}_3)(\text{CH}_2)_4(\text{NH}_3)]\text{CuCl}_4$ . The compound's thermal stability curve as per thermogravimetric analysis exhibits a stable state up to  $\sim 495$  K, while the weight loss observed near 538 K corresponds to partial thermal decomposition. The  $^1\text{H}$  nuclear magnetic resonance (NMR) chemical shifts for  $\text{NH}_3$  change more significantly with temperature than those for  $\text{CH}_2$ , because the organic cation motion is enhanced at both ends of the organic chain. The  $^{13}\text{C}$  NMR chemical shifts for the ' $\text{CH}_2$ -1' units of the chain show an anomalous change, and those for ' $\text{CH}_2$ -2' (units closer to  $\text{NH}_3$ ) are shifted sharply. Additionally, the  $^{14}\text{N}$  NMR spectra reflect the changes of local symmetry near  $T_C$  ( $=323$  K). Moreover, the  $^{13}\text{C}$   $T_{1\rho}$  values for  $\text{CH}_2$ -2 are smaller than those for  $\text{CH}_2$ -1, and the  $^{13}\text{C}$   $T_{1\rho}$  data curve for  $\text{CH}_2$ -1 exhibits an anomalous behaviour between 260 and 310 K. These smaller  $T_{1\rho}$  values at lower temperatures indicate that  $^1\text{H}$  and  $^{13}\text{C}$  in the organic chains are more flexible at these temperatures. The  $\text{NH}_3$  group is attached to both ends of the organic chain, and  $\text{NH}_3$  forms a  $\text{N}-\text{H}\cdots\text{Cl}$  hydrogen bond with the  $\text{Cl}$  ion of inorganic  $\text{CuCl}_4$ . When H and C are located close to the paramagnetic  $\text{Cu}^{2+}$  ion, the  $T_{1\rho}$  value is smaller than when these are located far from the paramagnetic ion.

Received 29th July 2020  
Accepted 13th September 2020

DOI: 10.1039/d0ra06551j

rsc.li/rsc-advances

## 1. Introduction

The search for new and improved functional materials in recent years has resulted in considerable progress in the synthesis of many families of organic–inorganic compounds. The properties and structural phase transition of these compounds are related to their structures and the interaction of the cationic units with complex anionic sublattices. One such group of hybrid compounds, whose structure can be expressed by the general formula  $[\text{NH}_3(\text{CH}_2)_4\text{NH}_3]\text{MX}_4$  ( $\text{M}$  = divalent metal ion and  $\text{X}$  = Cl, Br) is known to crystallise in a 2D perovskite-like structure, and these compounds are usually referred to as organic–inorganic hybrid perovskites or organic–metal-halide composites.<sup>1–6</sup> These perovskites combine the advantages of both organic and inorganic materials in a single molecular scale.<sup>1,7,8</sup> In particular, in the diammonium hybrid perovskite with its formula of  $[\text{NH}_3(\text{CH}_2)_4\text{NH}_3]\text{MX}_4$ , the  $\text{NH}_3$  group is attached to both ends of the organic chain.<sup>3,7,8</sup> At the end of the

organic part of the chain, the ammonium ion forms a  $\text{N}-\text{H}\cdots\text{X}$  hydrogen bond with the halide ion of the metallic inorganic layer.<sup>9</sup> These perovskite hybrids tend to exhibit a number of phase transitions such as order-disorder transitions. Here, we note that the properties of organic–inorganic hybrid perovskites depend on the organic cation, divalent metal, and halogen ion, and thus, it is necessary to investigate the 'structure-directing' properties of these new materials. In general, 2D hybrid perovskites can find use in the fields of energy, optoelectronics, photonics, and catalysis in green chemistry applications.<sup>9–13</sup>

The compound  $[(\text{NH}_3)(\text{CH}_2)_4(\text{NH}_3)]\text{CuCl}_4$ , or 1,4-butanediammonium tetrachlorocuprate, with  $\text{M} = \text{Cu}$  and  $\text{X} = \text{Cl}$ , undergoes a reversible phase transition at 325 K ( $=T_C$ )<sup>14</sup> between the two monoclinic phases II and I. The transition can be explained by order-disorder mechanisms involving a model of twisted conformation chains, which was introduced to explain the decrease in interlayer distance with increasing temperature from X-ray diffraction experiment. From structural considerations, these results can be explained by the conformational change of organic chains from the left-handed conformation in phase II to an all-trans conformation in phase I.<sup>14</sup> The structural geometry of  $[(\text{NH}_3)(\text{CH}_2)_4(\text{NH}_3)]\text{CuCl}_4$  in the room-temperature phase II and high-temperature phase I are represented in Fig. 1(a) and (b), respectively. The crystal structure at room temperature is monoclinic, corresponding to space group  $P2_1/c$ . The unit cell dimensions are  $a = 9.270$  Å,  $b = 7.600$  Å,  $c = 7.592$  Å,  $\beta = 103.14^\circ$ , and  $Z = 2$ .<sup>14,15</sup> Structural

<sup>a</sup>Department of Science Education, Jeonju University, Jeonju 55069, Korea. E-mail: aeranlim@hanmail.net; arlim@jj.ac.kr

<sup>b</sup>Department of Polymer Science and Engineering, Kumoh National Institute of Technology, Gumi 39177, Korea

<sup>c</sup>Analytical Laboratory of Advanced Ferroelectric Crystals, Jeonju University, Jeonju 55069, Korea

† Electronic supplementary information (ESI) available. See DOI: 10.1039/d0ra06551j



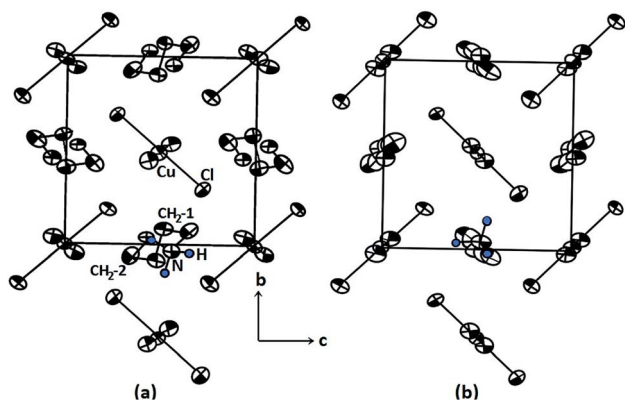


Fig. 1 Crystal arrangement on the *bc*-plane in  $[(\text{NH}_3)(\text{CH}_2)_4(\text{NH}_3)]\text{CuCl}_4$  for (a) room temperature phase II and (b) high temperature phase I. Here,  $\text{CH}_2\text{-1}$  represents two  $\text{CH}_2$  between four  $\text{CH}_2$ , and  $\text{CH}_2\text{-2}$  represents two  $\text{CH}_2$  close to  $\text{NH}_3$ .

cohesion is achieved *via*  $\text{N-H}\cdots\text{Cl}$  hydrogen bonds.  $[(\text{NH}_3)(\text{CH}_2)_4(\text{NH}_3)]\text{CuCl}_4$  is composed of alternating inorganic  $\text{CuCl}_4^{2-}$  layers and organic  $[\text{NH}_3(\text{CH}_2)_4\text{NH}_3]^{2+}$  sheets. The  $\text{CuCl}_4^{2-}$  layers are sandwiched by  $[\text{NH}_3(\text{CH}_2)_4\text{NH}_3]^{2+}$  cations, which possess centrosymmetrical chains with left-handed conformations at both ends, thereby forming the organic sheets. Above 325 K, the symmetry changes to that of a monoclinic structure with space group  $P2_1/c$ , and the corresponding lattice constants are  $a = 10.420 \text{ \AA}$ ,  $b = 7.442 \text{ \AA}$ ,  $c = 7.225 \text{ \AA}$ ,  $\beta = 93.46^\circ$ , and  $Z = 2$ .<sup>15</sup>

In the context of the property measurements of such compounds, Snively *et al.* conducted magnetic susceptibility measurements of  $[(\text{NH}_3)(\text{CH}_2)_4(\text{NH}_3)]\text{CuCl}_4$  powdered and single-crystals in the temperature range of 4 to 200 K.<sup>16,17</sup> They reported that the interplanar superexchange interaction along the linear  $\text{Cu-Cl-Cl-Cu}$  path exhibits a significantly stronger  $\text{Cu-Cu}$ -distance dependence than that along the  $\text{Cu-Cl-Cu}$  path. This crystal structure has been reported in phases I and II by Garland *et al.*<sup>18</sup> Subsequently, the phase transitions occurring in the perovskite-type 2D molecular composite  $[(\text{NH}_3)(\text{CH}_2)_4(\text{NH}_3)]\text{CuCl}_4$  have been studied by means of differential scanning calorimetry (DSC), X-ray diffraction (XRD),<sup>11</sup> and electron paramagnetic resonance (EPR).<sup>14,19,20</sup>

Understanding the structural dynamics of organic-inorganic hybrid perovskite  $[(\text{NH}_3)(\text{CH}_2)_4(\text{NH}_3)]\text{CuCl}_4$  is essential for their advanced use as new materials. Here, we study the structural dynamics of the organic-inorganic hybrid perovskite  $[(\text{NH}_3)(\text{CH}_2)_4(\text{NH}_3)]\text{CuCl}_4$  *via* magic angle spinning (MAS) nuclear magnetic resonance (NMR) and static NMR experiments. The chemical shifts and spin-lattice relaxation times in the rotating frame  $T_{1\rho}$  in the low- and high-temperature phases are measured by means of MAS  $^1\text{H}$  NMR and cross-polarisation (CP)/MAS  $^{13}\text{C}$  NMR to understand the role of the organic cation in this crystal. The  $^{14}\text{N}$  NMR spectra of the compound in the laboratory frame are also obtained as a function of temperature. We use these results to discuss the structural dynamics of the  $\text{NH}_3\text{-CH}_2\text{-CH}_2\text{-CH}_2\text{-CH}_2\text{-NH}_3$  chain below and above the phase transition temperature  $T_c$ . In particular, an

examination of the hydrogen bonding of  $\text{N-H}\cdots\text{Cl}$  between the  $\text{Cu-Cl}$  layer and the alkylammonium chain within  $[(\text{NH}_3)(\text{CH}_2)_4(\text{NH}_3)]\text{CuCl}_4$  can provide important insights into the operational mechanism as regards potential applications.

## II. Experimental method

Crystals of  $[(\text{NH}_3)(\text{CH}_2)_4(\text{NH}_3)]\text{CuCl}_4$  were prepared by mixing equimolar amounts of  $\text{NH}_2(\text{CH}_2)_4\text{NH}_2\cdot 2\text{HCl}$  and  $\text{CuCl}_2$  in aqueous solution and allowing the resulting mixture to slowly evaporate. The light-green-coloured crystals grew as rectangular parallelepipeds with dimensions of  $5 \text{ mm} \times 5 \text{ mm} \times 1 \text{ mm}$ .

The crystal structure of  $[(\text{NH}_3)(\text{CH}_2)_4(\text{NH}_3)]\text{CuCl}_4$  was determined with a X-ray diffraction system, using a  $\text{Cu-K}\alpha$  radiation source at the KBSI, Seoul Western Center. DSC (TA, DSC 25) experiments were carried out at a heating rate of  $10^\circ\text{C min}^{-1}$  in the temperature range of 190 to 600 K in a nitrogen-gas atmosphere. Thermogravimetry analysis (TGA) experiments were conducted using a thermogravimetric analyser (TA Instruments) under conditions identical to those of DSC over a temperature range of 300 to 680 K. The DSC and TGA experiments were performed by using crystal sample quantities of 6.23 and 7.53 mg, respectively.

Solid-state MAS NMR investigations of the  $[(\text{NH}_3)(\text{CH}_2)_4(\text{NH}_3)]\text{CuCl}_4$  crystals were conducted by using a 400 MHz Avance II+ Bruker NMR spectrometer at the same facility. The MAS  $^1\text{H}$  NMR and CP/MAS  $^{13}\text{C}$  NMR experiments were performed at the Larmor frequencies of  $\omega_0/2\pi = 400.13$  and  $100.61 \text{ MHz}$ , respectively. Solid samples were packed into 4 mm-diameter zirconia rotors and closed off using Vespel caps. The samples were spun at 10 kHz MAS by using dry nitrogen gas. The  $^1\text{H}$  and  $^{13}\text{C}$  NMR chemical shifts were obtained with the use of tetramethylsilane (TMS) as a standard. The  $T_{1\rho}$  data for  $^1\text{H}$  and  $^{13}\text{C}$  were obtained by applying a  $\pi/2$  pulse, immediately followed by a long spin-locking pulse phase-shifted by  $\pi/2$  with respect to the  $\pi/2$  pulse. The width of the  $\pi/2$  pulse used for  $T_{1\rho}$  measurements was  $3.3 \text{ }\mu\text{s}$ , which yields the frequency of the rotating frame as  $\omega_1 = 75.75 \text{ kHz}$ . The  $T_{1\rho}$  data were obtained by varying the length of the spin-locking pulse. In addition, the  $^{14}\text{N}$  NMR spectra of a  $[(\text{NH}_3)(\text{CH}_2)_4(\text{NH}_3)]\text{CuCl}_4$  single-crystal were obtained at the Larmor frequency of  $\omega_0/2\pi = 28.90 \text{ MHz}$  in the laboratory frame. The  $^{14}\text{N}$  resonance frequency was referenced with  $\text{NH}_3\text{NO}_3$  as the standard sample. The  $^{14}\text{N}$  NMR spectrum was obtained by the application of the following solid-state echo sequence:  $8 \text{ }\mu\text{s-tau}$  ( $16 \text{ }\mu\text{s}$ )– $8 \text{ }\mu\text{s-tau}$  ( $16 \text{ }\mu\text{s}$ ). The temperature change was maintained within the error range of  $\pm 0.5 \text{ K}$  by adjusting the nitrogen gas flow and heater current.

## III. Results and discussion

The powder X-ray diffraction pattern of  $[(\text{NH}_3)(\text{CH}_2)_4(\text{NH}_3)]\text{CuCl}_4$  at 300 K is described in the ESI,<sup>†</sup> and this data is consistent with previously reported results.<sup>14</sup> Fig. 2 shows the DSC curve of the  $[(\text{NH}_3)(\text{CH}_2)_4(\text{NH}_3)]\text{CuCl}_4$  crystals obtained with the heating rate of  $10^\circ\text{C min}^{-1}$ . An endothermic signal corresponding to the previously reported<sup>14</sup> II–I phase transition is detected at 323 K. In addition, a very large exothermic peak is



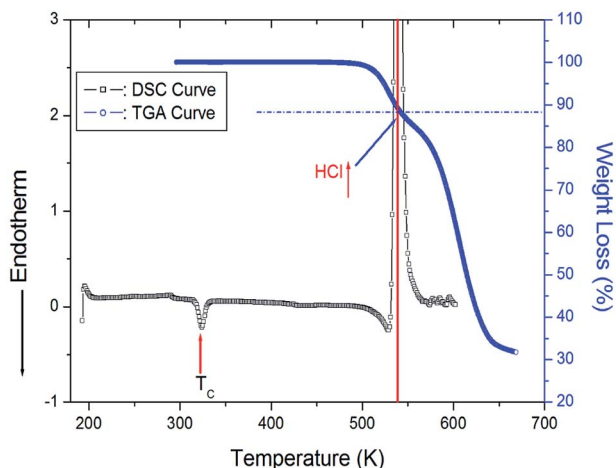


Fig. 2 Differential Scanning Calorimetry (DSC) and thermogravimetric analysis (TGA) curves of  $[(\text{NH}_3)(\text{CH}_2)_4(\text{NH}_3)]\text{CuCl}_4$ .

observed at 538 K. To understand the origins of this peak, we performed TGA experiments; these results are also shown in Fig. 2. In the TGA curve, a stable state is observed up to  $\sim 495$  K, whereas a weight loss is observed at higher temperatures, which represents partial thermal decomposition. Here, we note that  $[(\text{NH}_3)(\text{CH}_2)_4(\text{NH}_3)]\text{CuCl}_4$  crystals show the weight loss with temperature increase. From the TGA experimental results and possible chemical reactions, we compared the weight loss. The weight loss of 12% around 538 K obtained from the DSC experiment is consistent with the calculated decomposition of HCl moieties. From the figure, we note that the weight sharply decreases between 500 and 650 K, with a corresponding weight loss of 67% near 650 K.

Next, we acquired the MAS  $^1\text{H}$  NMR spectrum of the  $[(\text{NH}_3)(\text{CH}_2)_4(\text{NH}_3)]\text{CuCl}_4$  crystals at various temperatures (Fig. 3). In the figure, we can observe two resonance signals for  $^1\text{H}$ . The spinning sidebands corresponding to  $\text{CH}_2$  are indicated

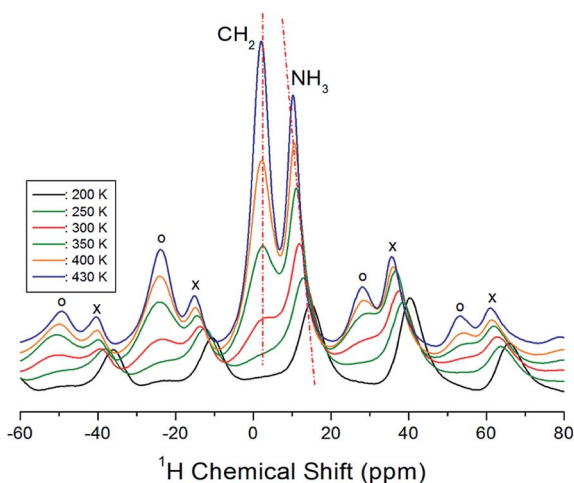


Fig. 3 MAS  $^1\text{H}$  NMR spectra for  $\text{CH}_2$  and  $\text{NH}_3$  of  $[(\text{NH}_3)(\text{CH}_2)_4(\text{NH}_3)]\text{CuCl}_4$  at various temperatures (spinning sidebands for  $\text{CH}_2$  and  $\text{NH}_3$  are indicated by open circles and crosses, respectively).

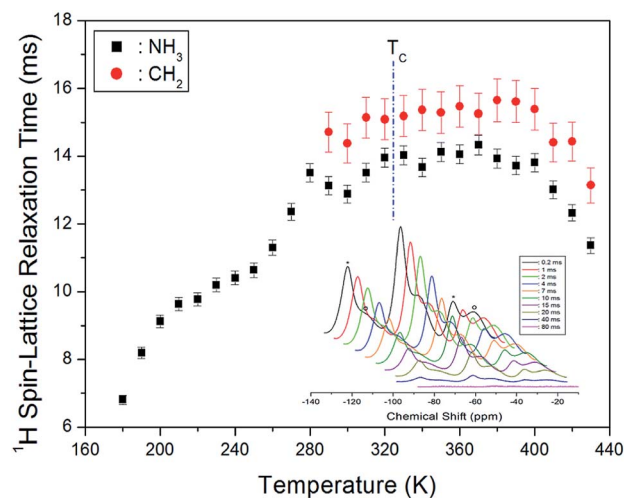


Fig. 4  $^1\text{H}$  NMR spin-lattice relaxation times  $T_{1\rho}$  for  $\text{CH}_2$  and  $\text{NH}_3$  ions of  $[(\text{NH}_3)(\text{CH}_2)_4(\text{NH}_3)]\text{CuCl}_4$  as a function of temperature (inset:  $^1\text{H}$  NMR spectrum at several delay times at 300 K).

by open circles, and those of  $\text{NH}_3$  are indicated by crosses. At 300 K, the  $^1\text{H}$  NMR chemical shifts for  $\text{CH}_2$  and  $\text{NH}_3$  are observed at  $\delta = 2.73$  ppm and  $\delta = 11.86$  ppm, respectively. Below 300 K, the  $^1\text{H}$  resonance signal bonded to  $\text{CH}_2$  mostly merges with the  $^1\text{H}$  resonance signal bonded to  $\text{NH}_3$ , which makes it difficult to distinguish the two signals. In addition, the  $^1\text{H}$  resonance signal for  $\text{CH}_2$  is related to the number of bonded protons, which means that the signal exhibits a stronger intensity and wider linewidth than the corresponding ones for  $\text{NH}_3$ . The  $^1\text{H}$  NMR chemical shifts according to the temperature exhibit a greater change for  $\text{NH}_3$  than  $\text{CH}_2$ . These results indicate that  $\text{NH}_3$  is temperature-sensitive.

Next, we measured the MAS  $^1\text{H}$  NMR spectrum at various temperatures, and the intensity change for the delay time was observed to obtain the spin-lattice relaxation time in the rotating frame ( $T_{1\rho}$ ) for  $^1\text{H}$  at each temperature. Normally, the  $T_{1\rho}$  data can be obtained as the slope of the intensity or the ratio of the area of the resonance signal to the delay time. The change in the proton magnetisation intensity in terms of  $T_{1\rho}$  is expressed as below:<sup>21–23</sup>

$$P(\tau) = P(0) \exp(-\tau/T_{1\rho}), \quad (1)$$

where  $P(\tau)$  and  $P(0)$  denote the signal intensities at time  $\tau$  and  $\tau = 0$ , respectively. Next, at 300 K, the MAS  $^1\text{H}$  NMR signals of  $\text{CH}_2$  and  $\text{NH}_3$  were plotted for various delay times in the range from 0.2 to 80 ms (Fig. 4); we note that the intensities of the  $^1\text{H}$  NMR signal as a function of the delay times exhibit considerable variation. From the slope of the intensity vs. delay time curve, the  $^1\text{H}$   $T_{1\rho}$  data of  $[(\text{NH}_3)(\text{CH}_2)_4(\text{NH}_3)]\text{CuCl}_4$  were obtained for  $\text{CH}_2$  and  $\text{NH}_3$  in the low-temperature phase II and high-temperature phase I. From Fig. 4, we note that no changes are observed in the  $T_{1\rho}$  value near  $T_c$ , and  $T_{1\rho}$  slightly increases according to the temperature change. The  $^1\text{H}$   $T_{1\rho}$  values for  $\text{CH}_2$  and  $\text{NH}_3$  at 300 K are 14.37 and 12.88 ms, respectively. Here, the  $^1\text{H}$   $T_{1\rho}$  value for  $\text{NH}_3$  is smaller than that for  $\text{CH}_2$ . This is



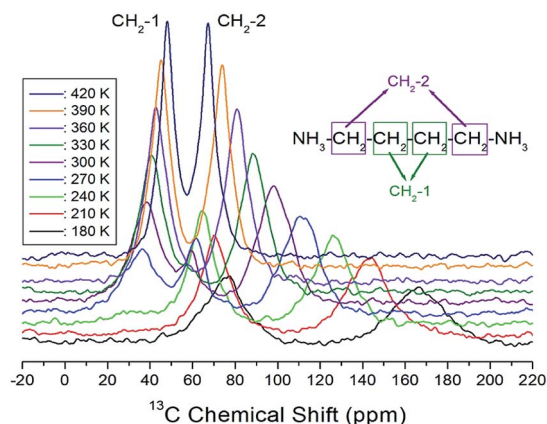


Fig. 5 *In situ* MAS  $^{13}\text{C}$  NMR spectra for  $\text{CH}_2\text{-1}$  and  $\text{CH}_2\text{-2}$  of  $[(\text{NH}_3)(\text{CH}_2)_4(\text{NH}_3)]\text{CuCl}_4$  as a function of temperature.

possibly because  $\text{NH}_3$  is closer to the inorganic  $\text{CuCl}_4$  layer; the  $T_{1\rho}$  value becomes smaller as the distance between H and the paramagnetic  $\text{Cu}^{2+}$  ion reduces. This is because  $T_{1\rho}$  is inversely proportional to the square of the magnetic moment of the paramagnetic ion.<sup>21</sup>

The CP/MAS  $^{13}\text{C}$  NMR chemical shifts measured at various temperatures are shown in Fig. 5. In the study, the MAS  $^{13}\text{C}$  NMR spectrum for TMS was recorded at 38.3 ppm at 300 K, and this value was calibrated to determine the chemical shift in  $^{13}\text{C}$ . Here, the two inner  $\text{CH}_2$  groups of the four  $\text{CH}_2$  ones are together designated as  $\text{CH}_2\text{-1}$ , and the two  $\text{CH}_2$  units close to the  $\text{NH}_3$  ones are designated as  $\text{CH}_2\text{-2}$ . We note from the figure that the  $^{13}\text{C}$  chemical shifts for  $\text{CH}_2\text{-1}$  (far from  $\text{NH}_3$ ) are different from those for  $\text{CH}_2\text{-2}$ , which is closer to  $\text{NH}_3$ . In the  $^{13}\text{C}$  NMR spectra obtained for  $\text{CH}_2\text{-1}$  and  $\text{CH}_2\text{-2}$ , two unusual resonance lines are observed between 260 and 310 K. At 300 K, the two resonance signals for  $\text{CH}_2\text{-1}$  are recorded at chemical shifts of  $\delta = 38.44$  and 59.56 ppm. Furthermore, the signal of  $\delta = 98.23$  ppm corresponds to  $\text{CH}_2\text{-2}$ . The  $^{13}\text{C}$  chemical shifts

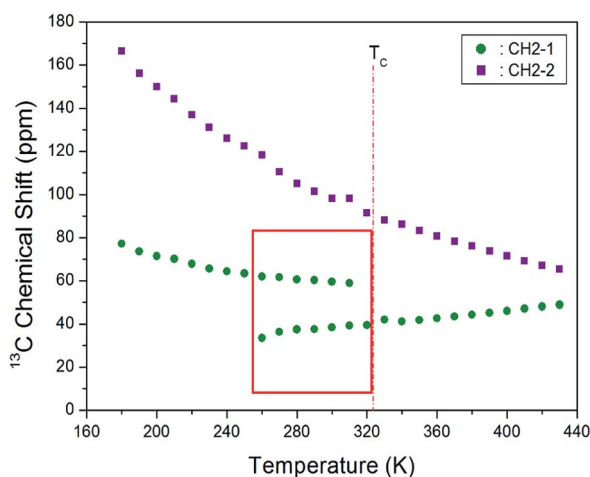


Fig. 6 MAS  $^{13}\text{C}$  chemical shifts for  $\text{CH}_2\text{-1}$  and  $\text{CH}_2\text{-2}$  of  $[(\text{NH}_3)(\text{CH}_2)_4(\text{NH}_3)]\text{CuCl}_4$  at low temperature phase II and high temperature phase I.

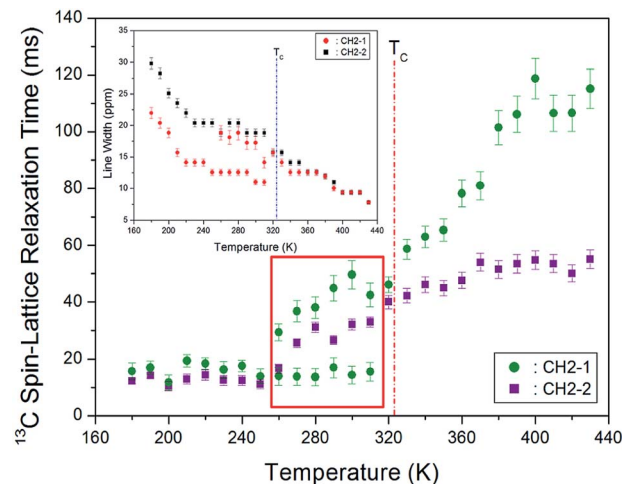


Fig. 7 MAS  $^{13}\text{C}$  NMR spin-lattice relaxation times  $T_{1\rho}$  for  $\text{CH}_2\text{-1}$  and  $\text{CH}_2\text{-2}$  of  $[(\text{NH}_3)(\text{CH}_2)_4(\text{NH}_3)]\text{CuCl}_4$  as a function of temperature (inset: line widths for  $\text{CH}_2\text{-1}$  and  $\text{CH}_2\text{-2}$  according to the temperature).

for  $\text{CH}_2\text{-1}$  exhibit an anomalous change with increase in temperature, whereas those for  $\text{CH}_2\text{-2}$  shift abruptly with increasing temperature, as shown in Fig. 6. The two resonance lines between 260 and 310 K correspond to  $\text{CH}_2\text{-1}$ , and hitherto unreported anomalous phenomena are observed in this temperature range.

We next remark that line broadening in the MAS  $^{13}\text{C}$  NMR spectra is influenced by relaxation processes such as the motional modulations of the chemical shift anisotropy and dipolar carbon-proton coupling. Fig. 7 shows the  $^{13}\text{C}$  full-width at half-maximum (FWHM) linewidth of  $[(\text{NH}_3)(\text{CH}_2)_4(\text{NH}_3)]\text{CuCl}_4$ . The  $^{13}\text{C}$  NMR line shapes vary from the Gaussian type at lower temperatures to the Lorentzian shape at higher temperatures. The appearance of these two-component spectra is caused by difference in different molecular motions. The line-width near the phase transition temperature  $T_c$  shows

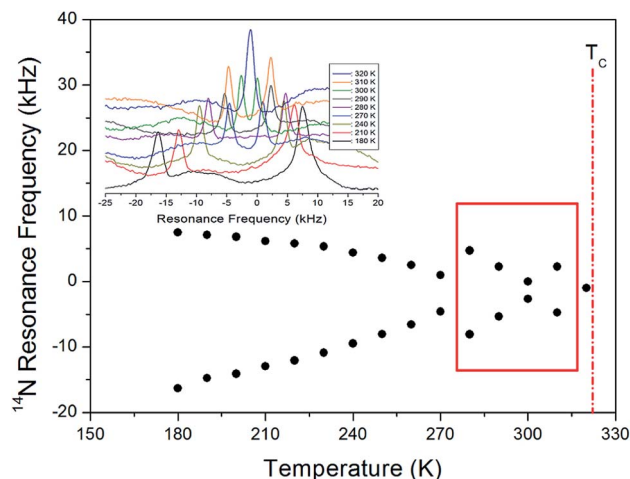


Fig. 8  $^{14}\text{N}$  resonance frequency of  $[(\text{NH}_3)(\text{CH}_2)_4(\text{NH}_3)]\text{CuCl}_4$  single crystal as a function of temperature (inset: *in situ*  $^{14}\text{N}$  resonance frequency at several temperatures).



**Table 1** Phase transition temperature  $T_C$ , decomposition temperature  $T_d$ , structure, space group, lattice constant, spin-lattice relaxation time  $T_{1\rho}$  for  $[\text{C}_2\text{H}_5\text{NH}_3]_2\text{CuCl}_4$  and  $[\text{NH}_3(\text{CH}_2)_4\text{NH}_3]\text{CuCl}_4$  crystals

	$[\text{C}_2\text{H}_5\text{NH}_3]_2\text{CuCl}_4$	$[\text{NH}_3(\text{CH}_2)_4\text{NH}_3]\text{CuCl}_4$
$T_C$ (K)	236, 330, 357, 371 (ref. 26–31)	325 (ref. 14)
$T_d$ (K)	430	495
Structure	Orthorhombic <sup>32–34</sup>	Monoclinic <sup>14,15</sup>
Space group	<i>Pbca</i>	<i>P2<sub>1</sub>/c</i>
Lattice constant (Å)	$a = 7.47$ $b = 7.35$ $c = 21.18$	$a = 9.270$ $b = 7.600$ $c = 7.592$ $\beta = 103.14^\circ$
$^1\text{H}$ $T_{1\rho}$ (ms)	7–20 (ref. 35)	6–16
$^{13}\text{C}$ $T_{1\rho}$ (ms)	2–200	10–120

a monotonic decrease, thereby indicating the presence of motional narrowing at high temperatures.

The spin–lattice relaxation time in the rate of relaxation is due to spin–lattice interactions in the rotating frame. The  $^{13}\text{C}$   $T_{1\rho}$  relaxations are not influenced by spin diffusion because of the small dipolar coupling which arises from the low natural abundance and large separation of the nuclei. Under these conditions, we next analysed differences in the chain motions. The integration change of the  $^{13}\text{C}$  NMR spectrum obtained for various delay times was measured, and all the decay curves for  $\text{CH}_2$ -1 and  $\text{CH}_2$ -2 were plotted by using a single exponential function. From the slope of their recovery traces, the  $^{13}\text{C}$   $T_{1\rho}$  data were obtained for  $\text{CH}_2$ -1 and  $\text{CH}_2$ -2 as a function of temperature, as shown in Fig. 7. It can be observed that although no change in the  $T_{1\rho}$  value is observed near  $T_C$ ,  $T_{1\rho}$  above  $T_C$  abruptly increases with increasing temperature. The  $^{13}\text{C}$   $T_{1\rho}$  values for  $\text{CH}_2$ -1 and  $\text{CH}_2$ -2 at lower temperatures (below  $T_C$ ) are nearly identical; however, the  $^{13}\text{C}$   $T_{1\rho}$  values for  $\text{CH}_2$ -2 close to  $\text{NH}_3$  at high temperatures are smaller than that for  $\text{CH}_2$ -1. At high temperatures, smaller  $^{13}\text{C}$   $T_{1\rho}$  values for  $\text{CH}_2$ -2 are more flexible than the  $\text{CH}_2$ -1. Just as the  $^{13}\text{C}$  resonance lines for  $\text{CH}_2$ -1 exhibited anomalies between 260 and 310 K, the  $^{13}\text{C}$   $T_{1\rho}$  also exhibits two different sets of values. The relaxation time for Arrhenius-type random motions with correlation time  $\tau_C$  is described in term of slow motions; for  $\tau_C \ll \omega_L$ ,  $T_{1\rho} \sim \tau_C = \tau_0 \exp(-E_a/k_B T)$ , where  $\omega_L$  denotes the Larmor frequency and  $E_a$  the activation energy.

The  $^{14}\text{N}$  NMR spectrum in the laboratory frame was next measured in the temperature range from 180 to 430 K by using the solid-state echo method at the Larmor frequency of 28.90 MHz by means of static NMR. The two resonance lines are obtained by spin number  $I = 1$ ,<sup>24,25</sup> and the resonance frequency around  $T_C$  ( $=323$  K) changes as shown in Fig. 8. The observed change in the  $^{14}\text{N}$  resonance frequency with temperature is due to structural geometry change, which means a change in the quadrupole coupling constant. The linewidth at 300 K is  $\sim 44$  ppm, and this spectrum is relatively broader than the  $^1\text{H}$  and  $^{13}\text{C}$  NMR spectra. The  $^{14}\text{N}$  resonance frequency decreases almost continuously until 270 K, while that of the  $^{14}\text{N}$  signal between 280 and 310 K exhibits an anomalous pattern. Similar to the anomaly of the  $^{13}\text{C}$  resonance line observed between 260

and 310 K, an abnormal phenomenon is observed in the  $^{14}\text{N}$  resonance line in this region. At 320 K near  $T_C$ , there is only one  $^{14}\text{N}$  resonance line, and at temperatures  $>320$  K, no resonance lines are observed. At the transition point of 323 K, the  $^{14}\text{N}$  NMR lines merge into one line. This single  $^{14}\text{N}$  resonance line indicates that there is no electric field gradient (EFG) tensor at the N site in phase I because of site symmetry. The EFG tensor changes around the N site, which indicates a change in the structural configuration around the N site near  $T_C$ .

## IV. Conclusions

In this study, we investigated the thermal behaviour and physical properties of organic–inorganic hybrid perovskite  $[(\text{NH}_3)(\text{CH}_2)_4(\text{NH}_3)]\text{CuCl}_4$  crystals. The structural dynamics of  $[(\text{NH}_3)(\text{CH}_2)_4(\text{NH}_3)]\text{CuCl}_4$  with emphasis on the role of the  $[(\text{NH}_3)(\text{CH}_2)_4(\text{NH}_3)]$  cation, were discussed by MAS  $^1\text{H}$  NMR, MAS  $^{13}\text{C}$  NMR, and static  $^{14}\text{N}$  NMR as a function of temperature. Firstly, we found that the TGA curve exhibited stability until 495 K, and the observed weight loss of 12% near 538 K was due to the partial thermal decomposition of HCl moieties.

Secondly, the  $^1\text{H}$  NMR chemical shift of  $\text{NH}_3$  for crystallographic environments changed more significantly with temperature than that for  $\text{CH}_2$  because the  $[(\text{NH}_3)(\text{CH}_2)_4(\text{NH}_3)]$  cation motion is enhanced at both ends of the cation of the  $\text{NH}_3$  group. The  $^{13}\text{C}$  NMR chemical shifts for  $\text{CH}_2$ -1 showed an anomalous change, and those for  $\text{CH}_2$ -2 shifted sharply to lower values when compared with that of  $\text{CH}_2$ -1. The  $^{13}\text{C}$  chemical shifts of the  $\text{CH}_2$ -2 unit (closer to the  $\text{N}-\text{H}\cdots\text{Cl}$  bond) sharply changed relative to those of  $\text{CH}_2$ -1. In addition, the  $^{14}\text{N}$  NMR spectra reflected the changes in the local symmetry of the crystal near  $T_C$ .

The  $^1\text{H}$   $T_{1\rho}$  values for  $\text{CH}_2$  and  $\text{NH}_3$  slightly increased with temperature increase. Moreover, the  $^{13}\text{C}$   $T_{1\rho}$  value for  $\text{CH}_2$ -2 was smaller than that of  $\text{CH}_2$ -1, and the  $^{13}\text{C}$   $T_{1\rho}$  value for  $\text{CH}_2$ -1 exhibited an anomalous trend between 260 and 310 K. At low temperatures, the  $^1\text{H}$  and  $^{13}\text{C}$   $T_{1\rho}$  values were smaller than at high temperatures. Smaller  $T_{1\rho}$  values at lower temperatures indicate that  $^1\text{H}$  and  $^{13}\text{C}$  in the organic chains are more flexible at these temperatures. Moreover, the  $^{13}\text{C}$  of  $\text{CH}_2$ -2 close to  $\text{NH}_3$  of the organic chain is more flexible than the  $^{13}\text{C}$  of  $\text{CH}_2$ -1



between the four CH<sub>2</sub> sites. The NH<sub>3</sub> group is attached to both ends of the organic chain, and it forms a N–H···Cl hydrogen bond with the Cl ion of the inorganic CuCl<sub>4</sub>. The  $T_{1\rho}$  value is smaller when H and C are located close to the paramagnetic Cu<sup>2+</sup> ion than when far away. Additionally, the NH<sub>3</sub> groups are coordinated by CuCl<sub>4</sub>, and thus, atomic displacements in the environment of the <sup>14</sup>N nuclei with temperature are correlated with CuCl<sub>4</sub>. We also note here that detailed studies are required to examine the anomalies observed in the range of 260 to 310 K.

Here, we compared the phase transition temperatures, decomposition temperatures, crystal structures, space groups, lattice constants, and spin-lattice relaxation times of the previously reported [C<sub>2</sub>H<sub>5</sub>NH<sub>3</sub>]<sub>2</sub>CuCl<sub>4</sub> (ref. 26–35) and those of [NH<sub>3</sub>(CH<sub>2</sub>)<sub>4</sub>NH<sub>3</sub>]<sub>2</sub>CuCl<sub>4</sub> examined in this study; this is summarised in Table 1. The difference between the two crystals is only the presence of organic cation. The two compounds have four and one phase transition temperatures, respectively. The decomposition temperature of [NH<sub>3</sub>(CH<sub>2</sub>)<sub>4</sub>NH<sub>3</sub>]<sub>2</sub>CuCl<sub>4</sub> is higher than that of [C<sub>2</sub>H<sub>5</sub>NH<sub>3</sub>]<sub>2</sub>CuCl<sub>4</sub>, and the [NH<sub>3</sub>(CH<sub>2</sub>)<sub>4</sub>NH<sub>3</sub>]<sub>2</sub>CuCl<sub>4</sub> has a high thermal stability. Furthermore, the <sup>1</sup>H and <sup>13</sup>C  $T_{1\rho}$  values in [C<sub>2</sub>H<sub>5</sub>NH<sub>3</sub>]<sub>2</sub>CuCl<sub>4</sub> are slightly different from those for [NH<sub>3</sub>(CH<sub>2</sub>)<sub>4</sub>NH<sub>3</sub>]<sub>2</sub>CuCl<sub>4</sub>. Although the two crystals have same anions, the molecular motions according to the <sup>13</sup>C bond lengths of the (C<sub>2</sub>H<sub>5</sub>NH<sub>3</sub>) cation in [C<sub>2</sub>H<sub>5</sub>NH<sub>3</sub>]<sub>2</sub>CuCl<sub>4</sub> and [NH<sub>3</sub>(CH<sub>2</sub>)<sub>4</sub>NH<sub>3</sub>]<sub>2</sub>CuCl<sub>4</sub> are different. The above results suggest that the molecular motions obtained from <sup>1</sup>H and <sup>13</sup>C  $T_{1\rho}$  will be considered as good examples of potential applicability.

## Conflicts of interest

There are no conflicts to declare.

## Acknowledgements

This research was supported by the Basic Science Research program through the National Research Foundation of Korea, funded by the Ministry of Education, Science, and Technology (grant numbers 2018R1D1A1B07041593 and 2016R1A6A1A03012069).

## References

- 1 S. Gonzalez-Carrero, R. E. Galian and J. Perez-Prieto, *Part. Part. Syst. Charact.*, 2015, **32**, 709.
- 2 W. Liu, J. Xing, J. Zhao, X. Wen, K. Wang, L. Peixiang and Q. Xiong, *Adv. Opt. Mater.*, 2017, **5**, 1601045.
- 3 M. F. Mostafa, S. S. El-khiyami and S. K. Abdel-Aal, *J. Mol. Struct.*, 2017, **1127**, 59.
- 4 P. Mondal, S. K. Abdel-Aal, D. Das and S. K. Manirul Islam, *Catal. Lett.*, 2017, DOI: 10.1007/s10562-017-2112-7.
- 5 S. K. Abdel-Aal, *Solid State Ionics*, 2017, **303**, 29.
- 6 M. Yuan, L. N. Quan, R. Comin, G. Walters, R. Sabatini, O. Voznyy, *et al.*, *Nat. Nanotechnol.*, 2016, **11**, 872.
- 7 Z. Cheng and J. Lin, *CrystEngComm*, 2010, **12**, 2646.
- 8 D. B. Mitzi, *Chem. Mater.*, 1996, **8**, 791.
- 9 S. K. Abdel-Aal, G. Kocher-Oberlehner, A. Ionov and R. N. Mozhchil, *Appl. Phys. A*, 2017, **123**, 531.
- 10 S. K. Abdel-Aal and A. S. Abdel-Rahman, *J. Cryst. Growth*, 2017, **457**, 282.
- 11 A. M. Al-Amri, S.-F. leung, M. Vaseem, A. Shamim and J.-H. He, *IEEE Trans. Electron Devices*, 2019, **66**, 2657.
- 12 A. M. Al-Amri, B. Cheng and J.-H. He, *IEEE Trans. Nanotechnol.*, 2019, **18**, 1.
- 13 C.-H. Lin, C.-Y. Kang, T.-Z. Wu, C.-L. Tsai, C.-W. Sher, X. Guan, P.-T. Lee, T. Wu, C.-H. Ho, H.-C. Kuo and J.-H. He, *Adv. Funct. Mater.*, 2010, **30**, 1909275.
- 14 T. Maris, N. B. Chanh, J.-C. Bissey, N. Filloleau, S. Flandrois, R. Zouari and A. Daoud, *Phase Transitions*, 1998, **66**, 81.
- 15 T. Maris, G. Bravic, N. B. Chanh, J. M. Leger, J. C. Bissey, A. Villesuzanne, R. Zouari and A. Daoud, *J. Phys. Chem. Solids*, 1996, **57**, 1963.
- 16 L. O. Snively, G. F. Tuthill and J. E. Drumheller, *Phys. Rev. B: Condens. Matter Mater. Phys.*, 1981, **24**, 5349.
- 17 L. O. Snively, J. E. Drumheller and K. Emerson, *Phys. Rev. B: Condens. Matter Mater. Phys.*, 1981, **23**, 6013.
- 18 J. K. Garland, K. Emerson and M. R. Pressprich, *Acta Crystallogr., Sect. C: Cryst. Struct. Commun.*, 1990, **46**, 1603.
- 19 J.-C. Bissey, R. Berger, P. Beziade, N.-B. Chanh, T. Maris, R. Zouari and A. Daoud, *Solid State Commun.*, 1996, **97**, 669.
- 20 T. M. Kite, J. E. Drumheller and K. Emerson, *J. Magn. Reson.*, 1982, **48**, 20.
- 21 A. Abragam, *The Principles of Nuclear Magnetism*, Oxford University press, 1961.
- 22 J. L. Koenig, *Spectroscopy of Polymers*, Elsevier, New York, 1999.
- 23 R. K. Harris, *Nuclear Magnetic Resonance Spectroscopy*, Pitman Pub., UK, 1983.
- 24 J. Seliger, R. Blinc, H. Arend and R. Kind, *Z. Physik B*, 1976, **25**, 189.
- 25 S. Mulla-Osman, D. Michel and Z. Czaplá, *Phys. Status Solidi B*, 2003, **236**, 173.
- 26 V. Kapustianyk, V. Rudyk and M. Partyka, *Phys. Status Solidi B*, 2007, **244**, 2151.
- 27 V. B. Kapustianik, V. V. Bazhan and Yu. M. Korchak, *Phys. Status Solidi B*, 2002, **234**, 674.
- 28 W. Kleemann, F. J. Schafer, E. Karajamaki, R. Laiho and T. Levola, *Physica B*, 1983, **119**, 269.
- 29 V. Kapustianik, Yu. Korchak, I. Polovinko, R. Tchukvinskyi, Z. Czaplá and S. Dacko, *Phys. Status Solidi B*, 1998, **207**, 95.
- 30 C. B. . Mohamed, K. Karoui, F. Jomni, K. Guidara and A. B. . Rhaïem, *J. Mol. Struct.*, 2015, **1082**, 38.
- 31 I. R. Jahn, K. Knorr and J. Ihringer, *J. Phys.: Condens. Matter*, 1989, **1**, 6005.
- 32 B. Kundys, A. Lappas, M. Viret, V. Kapustianyk, V. Rudyk, S. Semak, Ch. Simon and I. Bakaimi, *Phys. Rev. B: Condens. Matter Mater. Phys.*, 2010, **81**, 224434.
- 33 P. Zolfaghari, G. A. de Wijs and R. A. de Groot, *J. Phys.: Condens. Matter*, 2013, **25**, 295502.
- 34 J. P. Steadman and R. D. Willett, *Inorg. Chim. Acta*, 1970, **4**, 367.
- 35 A. R. Lim and Y. L. Joo, *RSC Adv.*, 2018, **8**, 34110.

